J Mater Sci (2010) 45:5124–5134
DOI 10.1007/s10853-010-4579-0

ICAM 2009

Computer simulation study of amorphous compounds: structural and vibrational properties

Gonzalo Gutiérrez · Eduardo Menéndez-Proupin · Claudia Loyola · Joaquín Peralta · Sergio Davis

Received: 30 November 2009 / Accepted: 28 April 2010 / Published online: 15 May 2010

Abstract Molecular dynamic (MD) simulations, both classical and ab initio, of amorphous GeO_2 (germania), Al_2O_3 (alumina), and CdTeO compounds are presented. We focus our attention on the structural and vibrational properties, giving an atomic description of the short- and intermediate-range order. Amorphous germanium oxide under pressure was studied by means of classical MD simulations. At normal density, the analysis of the interatomic distances reveals that in the amorphous state there is a short-range order dominated by a slightly distorted (GeO_4) tetrahedron. Beyond that, there is an intermediate-range order composed by vertex-sharing tetrahedra. As density increases, there is a structural transformation, from a short-range order defined by the basic tetrahedron to a basic octahedron. Consistent with this picture, the vibrational density of states also presents big changes, where the low frequency band shrinks, and the high frequency becomes wider and flatter. In the case of alumina, both classical and first principles MD calculations of amorphous Al_2O_3 are reported, comparing both methodologies. Interatomic correlations allow us to conclude that the short-range order is mainly composed by AlO_4 tetrahedra, but in contrast to classical MD results, also an important number of AlO_5 unit is present. The vibrational density of states presents two main bands, a low frequency one related to the inter-tetrahedron vibration and a high frequency band related to the intra-tetrahedron vibration. Finally, we present an ab initio MD calculation for the complex ternary material $CdTeO_3$. According our calculations, the short-range order of this compound consists of a number of basic building blocks, greater than in the case of its crystalline counterpart. The compound is characterized using pair and angular distribution functions, coordination numbers, and a description of the molecular units of the compound. For example, Cd is coordinated by either six or five atoms. In the case of Te, the chemical unit is TeO_3. The most frequent clusters are CdO_6, CdO_5, TeO_3, and TeO_4.

G. Gutiérrez (✉) · E. Menéndez-Proupin · C. Loyola · J. Peralta · S. Davis
Group of NanoMaterials, Departamento de Física, Facultad de Ciencias, Universidad de Chile, Casilla 653, Santiago, Chile
e-mail: gonzalo@fisica.ciencias.uchile.cl

Introduction

Amorphous compounds, or glasses, are very important materials from the practical, experimental, and theoretical point of view [1, 2]. Amorphous materials have a wide range of applications, from windows, electronic devices (like cell phones) to optical coatings, MOSFET, opto-electronic technology, among others. In most of these applications, it is desirable to have an atomic level description of the material and its relation to the macroscopic properties. Unfortunately, because of the lack of long-range order in glasses, the experimental determination of their structural and dynamical properties is difficult. Diffraction experiments supply knowledge of interparticle distances but not of spatial arrangements. Also, there are problems with sample characterization. Some important disordered systems, like amorphous semiconductors, are not in thermodynamic equilibrium, i.e., they are not uniquely defined by their composition, temperature, and pressure. Their history and method of preparation can play a considerable part in determining their properties [3].

From the theoretical point of view, amorphous materials present a challenge due to several interesting features: for example, simplifying concepts, such as crystalline order leading to Bloch' s theorem in solid state physics or almost

perfect randomness leading to kinetic theory of gases, are not available for these systems. A determination of the structure of a crystalline solid is straightforwardly made by only solving the structure within the unit cell, which in most cases contains only a few atoms and is the fundamental building block of the structure. Such a procedure is impossible in amorphous materials, for which the unit cell may be regarded as being infinite in extent and specific to each sample. In fact, it is impossible to solve exactly the structure since the atoms can be arranged in an infinite number of ways. The best one can achieve is an average model of the system, which agrees reasonably well with all kind of experiments. Thus, the atomic arrangement in amorphous solids (like in liquids) is commonly described by statistical distribution functions such as the atomic pair distribution functions, the bond angle distribution, and rings distribution, which are one-dimensional representations of the real three-dimensional structures averaged over all atoms. However, it is difficult to obtain these statistical data for real systems. Nowadays, this task is undertaken by computer modeling, where MD techniques play a key role (for an update description of the computer simulation methods applied to amorphous materials, see the review of Drabold [4]).

In this article, we review our investigations in oxide glasses by computer simulation. In particular, via MD, both classical and ab initio, amorphous GeO_2 (germania), Al_2O_3 (alumina), and CdTeO compounds are studied, contrasting the results to their crystalline phases. We focus our attention on the structural and vibrational properties giving an atomic description of the short- and intermediate-range order.

Amorphous germanium oxide (GeO_2), a structural and chemical analog to silica (SiO_2), is an example of a covalent glass, and a good empirical pair-wise interatomic potential to be used in computer simulation exists. In order to investigate the structural transformation under pressure, we perform MD simulations in the microcanonical ensemble, with systems at densities ranging from 3.6 to 6.3 g/cm^3. The network topology of our system is analyzed through partial pair correlations, coordination number, and angle distributions, whereas the vibrational properties were characterized by means of the density of states. At normal density, a detailed analysis of the interatomic distances reveals that in the amorphous state there is a short-range order dominated by a slightly distorted (GeO_4) tetrahedron. Beyond that, there is an intermediate-range order composed by vertex-sharing tetrahedra. The vibrational density of states has two bands, a low frequency one up to 20 THz, and a high frequency band from 20 to 30 THz. As density increases, there is a structured transformation, from a short-range order defined by the basic tetrahedron (GeO_4) to a basic octahedron (GeO_6). Consistent with this picture, the vibrational density of states also presents big changes, where the low frequency band shrinks and the high frequency becomes wider and flatter.

In the case of alumina, both classical and first principles (also called ab initio) MD calculations of amorphous Al_2O_3 in a system consisting of a supercell of 80 atoms is reported. Our aim is to contrast both kinds of simulation. A detailed analysis of the interatomic correlations allows us to conclude that the short-range order is mainly composed by AlO_4 tetrahedra, but in contrast to classical MD results, also an important number of AlO_5 units are present in the ab initio MD simulation. The vibrational density of states, obtained as the Fourier transform of the velocity autocorrelation function, presents two main bands, a low frequency one related to the inter-tetrahedron vibration and a high frequency band related to the intra-tetrahedron vibration.

Finally, we present an ab initio MD calculation for the complex ternary material $CdTeO_3$. This compound, obtained in the form of amorphous thin films, has been grown by means of r.f. sputtering during the last decade, and has been playing an important role in solar cell technologies. Owing to the several different structural units present in CdTeO compounds, it is difficult to fit an empirical potential, and therefore, a parameter free calculation, like ab initio MD, is especially well suited. In this study we predict the short-range order of this compound and compare it to its crystalline counterpart. The compound is characterized using pair and angular distribution functions, coordination numbers, and a description of its molecular units.

This article is organized as follows: in section "Methods" we discuss the methods used. In section "Results" we present the results and discussion, and finally in section "Conclusions" we drawn the conclusions.

Methods

In the MD approach, the phase space trajectories of the system (positions, velocities of all atoms at all time) are obtained by solving numerically the equation of motion of the system [5, 6]. Thus, atoms (or molecules) are treated as classical particles which obey Newton's equations of motion. The interatomic forces can be obtained by means of empirical potentials (the so-called "classical MD") or by means of quantum mechanical calculation, via the Hellman–Feyman theorem ("ab initio" or "first principles MD").

In the case of classical MD, the interatomic force law for describing how atoms interact with each other is mathematically encoded in the interatomic potential energy, $V(\mathbf{r}_1, \ldots, \mathbf{r}_N)$, which is a function of the positions of all

N atoms, $\mathbf{r}_1$, $\mathbf{r}_2$, ..., $\mathbf{r}_N$, in the system. The empirical potential has a specific functional form, depending on the material under simulation, and its parameters are fitted with respect to experimental data or a precise quantum mechanical calculation. In our case, for GeO_2 for example, we use a pair-wise interatomic potential of the form

$$V(r_{ij}) = \frac{q_i q_j}{r_{ij}} - \frac{A_{ij}}{r_{ij}^6} + B_{ij}\exp\left(-C_{ij} r_{ij}\right), \tag{1}$$

where the terms represent Coulomb, van der Waals, and repulsion energies, respectively. Here r_{ij} is the interatomic distance between atoms i and j, and the effective charges q_i are $q_{\mathrm{Ge}} = 1.5$ and $q_{\mathrm{O}} = -0.75$. The van der Waals coefficients A_{ij}, the softness parameter B_{ij}, and the repulsive radius C_{ij} are the energy parameters [7].

Empirical potential simulations sometimes fail to describe certain properties of the systems. For instance, they cannot describe chemical processes. Instead, interatomic interaction in reactive regions needs to be calculated by quantum mechanical methods, able to describe breaking and formation of bonds. In this scheme, an atom consists of a nucleus and surrounding electrons, and quantum mechanics explicitly treats valence electrons whereas the movement of the ions (nucleus plus core electrons) is treated as a classical particle, exactly like classical MD. Since each electronic wave function is a linear combination of many states, the combinatorial solution space for the many-electron problem is exponentially large [8]. The density functional theory (DFT) avoids the exhaustive enumeration of many-electron correlations by solving M single-electron problems in a common average environment (M is the number of independent wave functions). As a result, the problem is reduced to a self-consistent matrix eigenvalue problem, which can be solved with $O(M^3)$ operations. Thus, at the end one obtains the ground state energy E of the system in a self-consistent way, where the ionic coordinates enter as parameters, that is, $E = E(\mathbf{R}_1, \ldots, \mathbf{R}_N)$, where N is the number of atoms of the system. The force on each atom is obtained by taking the appropriate derivative over the ground state energy, using the Feynman–Hellmann theorem, $\mathbf{F}_i = \langle\phi|\nabla_{\mathbf{R}_i} E|\phi\rangle$, where $|\phi\rangle$ is the electronic wave function. Now, one can use this force to move the ions, like in classical MD [9]. Note that ab initio MD, in contrast to classical MD, severely limits the size (number of particles) and total running time of the simulation, because it is very time consuming.

The physical properties are obtained by taking average over configurations, using the techniques of statistical mechanics, provided the ergodic hypothesis holds. In this way, one can calculate structural and dynamical properties. For example, basic information about structural correlations is derived from the partial pair distribution functions $g_{\alpha\beta}$ (PDF). In a multicomponent system these are determined from

$$g_{\alpha,\beta}(r) = \frac{\langle n_{\alpha,\beta}(r, r+\Delta r)\rangle}{4\pi r^2 \Delta r}\frac{V}{N_\beta}, \tag{2}$$

where $\langle n_{\alpha,\beta}(r, r+\Delta r)\rangle$ denotes the average number of particles of species β surrounding a particle of species α in a spherical shell between r and $r + \Delta r$ and N_β is the total number of particles of species β (being $N = \sum_\alpha N_\alpha$ the total number of particles in the system). The total pair distribution function is obtained from

$$g(r) = \sum_\alpha \sum_\beta c_\alpha c_\beta g_{\alpha\beta}(r), \tag{3}$$

where $c_{\alpha(\beta)} = N_{\alpha(\beta)}/N$ is the concentration of $\alpha(\beta)$ species.

Also, the coordination numbers and the angular distribution can be obtained directly from the coordinates of the different atomic configurations. The average coordination number $n_{\alpha\beta}$ is obtained by integration around the first peak in the partial pair distribution function, $n_{\alpha(\beta)}(R) = 4\pi\rho_\beta \int_0^R g_{\alpha\beta}(r) r^2 \mathrm{d}r$, where R is a cut-off radius, usually chosen as the position of the minimum after the first peak of $g_{\alpha\beta}(r)$.

Interestingly, MD results can be directly compared to experiment via the scattering structure factor. For example, the partial static structure factors are calculated from the Fourier transform of the corresponding partial PDF by means of

$$S_{\alpha\beta}(q) = \delta_{\alpha\beta} + 4\pi\rho(c_\alpha c_\beta)^{1/2} \times \int_0^R r^2[g_{\alpha\beta}(r) - 1]\frac{\sin(qr)}{qr}\frac{\sin(\pi r/R)}{\pi r/R}\mathrm{d}r, \tag{4}$$

where $c_{\alpha(\beta)} = N_{\alpha(\beta)}/N$ is the concentration of $\alpha(\beta)$ species. The window function $\frac{\sin(\pi r/R)}{\pi r/R}$ has been introduced to reduce the termination effects resulting from the finite upper limit [10]. The cut-off length, R, is chosen to be half the length of the simulation box.

Similarly, the neutron scattering static structure factor can be obtained from the partial static structure factors by weighting them with the coherent neutron scattering lengths:

$$S_N(q) = \frac{\sum_{\alpha\beta} b_\alpha b_\beta (c_\alpha c_\beta)^{1/2}[S_{\alpha\beta}(q) - \delta_{\alpha\beta} + (c_\alpha c_\beta)^{1/2}]}{\left(\sum_\alpha b_\alpha c_\alpha\right)^2}. \tag{5}$$

where b_α denotes the coherent neutron scattering length of species α.

Regarding the dynamical properties, the vibrational density of states $\mathcal{D}(\omega)$, for example, can be obtained by first calculating the velocity autocorrelation function for species α,

$$Z_\alpha(t) = \left\langle \sum_{i=1}^{N} m_{i\alpha}\mathbf{v}_{i\alpha}(t_0)\cdot\mathbf{v}_{i\alpha}(t_0+t)\right\rangle_{t_0}, \quad (6)$$

where $m_{i\alpha}$ is the mass of the atom i and species α, $\mathbf{v}_{i\alpha}$ its velocity, and <…> means average over different configurations. By performing a Fourier transform,

$$\mathcal{D}_\alpha(\omega) = \frac{1}{\sqrt{2\pi}}\int \frac{Z_\alpha(t)}{Z_\alpha(0)}\exp(-i\omega t)dt, \quad (7)$$

the partial $\mathcal{D}_\alpha(\omega)$ is obtained. From this, we obtain the total density of states, $\mathcal{D}(\omega) = \sum_\alpha c_\alpha \mathcal{D}_\alpha(\omega)$ and the total neutron section-weighted one phonon density of states [11],

$$\mathcal{D}_N(\omega) = \sum_\alpha \frac{c_\alpha 4\pi b_\alpha^2}{m_\alpha}\mathcal{D}_\alpha(\omega). \quad (8)$$

In this study, most of the analysis has been performed using our in-house code, *Las Palmeras Molecular Dynamics* (LPMD) [12].

Results

The atomic level study of amorphous GeO_2, Al_2O_3, and $CdTeO_3$ is done by analyzing the interatomic correlations such as PDF, coordination numbers, angular distributions, as well as the vibrational density of states calculated from the velocity autocorrelation function. Also, we employ visual inspection from snapshots or animations to clarify some aspects.

Amorphous GeO_2 under pressure

Germanium dioxide GeO_2, or germania, is a chemical and structural analog to silica (SiO_2), exhibiting similarities in many structural and physical properties. In crystalline state, germania has two phases: one low density phase (4.28 g/cm^3) with a quartz structure (Ge coordinated with four oxygen atoms) and a high-density phase (6.25 g/cm^3) with rutile structure (Ge coordinated with six oxygen atoms). In the amorphous state both, silica and germania, can be described as a continuous network of $A(O_{1/2})_4$ (A = Si, Ge) apex-bridged tetrahedra joined to each other by oxygen atoms.

When submitted to high pressure, both systems present a structural transition from a tetrahedral to an octahedral $A(O_{1/3})_6$, network, which implies a large change in density and in the short- and medium-range order [13]. But in contrast to amorphous silica, where such transformation occurs around 20 GPa, in amorphous germania it takes place between 5 and 9 GPa, which is more manageable in actual experiments.

In this study, we study the structural transformation of amorphous germania under pressure, using the same methodology as reference [14], that is, the NVE ensemble with 576 atoms, but obtaining 26 systems at room temperature, at densities ranging from 3.16 to 6.79 g/cm^3. Here we present detailed results for four systems, whose densities are 3.60, 4.86, 5.91, and 6.33 g/cm^3, which corresponds to pressure of −0.7, 2.5, 7.12, and 19.6 GPa, respectively. The interatomic potential employed is the one due to Oeffner and Elliot [7] described in Eq. 1, which was successfully used in a previous study to determine the structural and dynamical properties of GeO_2 at room pressure [14]. The long-range Coulomb interactions are calculated with the standard Ewald summation technique. The equations of motion are integrated with a modification of the Beeman algorithm, as is implemented in the program MOLDY [15], using a time step $\Delta t = 1 \times 10^{-15}$ s.

In Fig. 1 we present a comparison between MD and the experimental results. It can be seen that the agreement of the calculated and experimental neutron $S(q)$ is quite good. Only a small difference at the first peak is found, where the calculated one is slightly shifted to the right. In both figures, corresponding to $S_N(q)$ and $S_X(q)$, for $q \leq 5$ Å^{-1}, three main peaks—the first one at $q \sim 1.6$ Å^{-1}, a second one at $q \sim 2.6$ Å^{-1}, and a third one at $q \sim 4.5$ Å^{-1}—are observed. The second peak has a rather small intensity in comparison to the other two peaks.

Figure 2 presents the equation of state, which gives an overview of the simulation we performed. It can be seen that, as the specific volume decreases (from right to left in the plot), the pressure monotonically increases, up to a point (near 0.19 cm/g^3) where this trend finishes. Then, 0.19–0.17 cm/g^3, there is a valley, and after that, the pressure begins to increase again, but with a more pronounced slope. This picture is a fingerprint of a structural transformation. As we will see by an atomic level analysis,

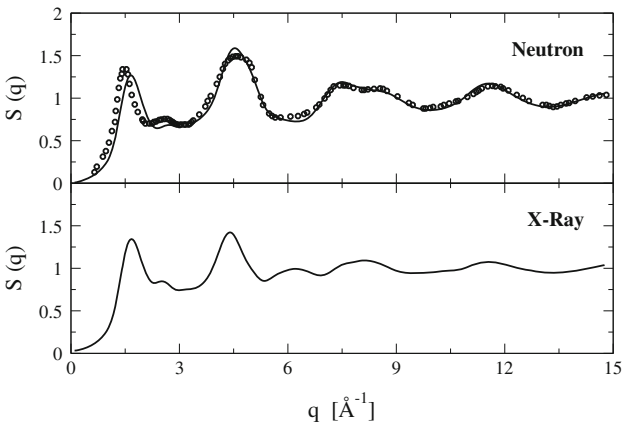

Fig. 1 Neutron and X-ray structure factors for amorphous GeO_2. *Dot* indicates experimental result [16] and *full line* our MD simulation

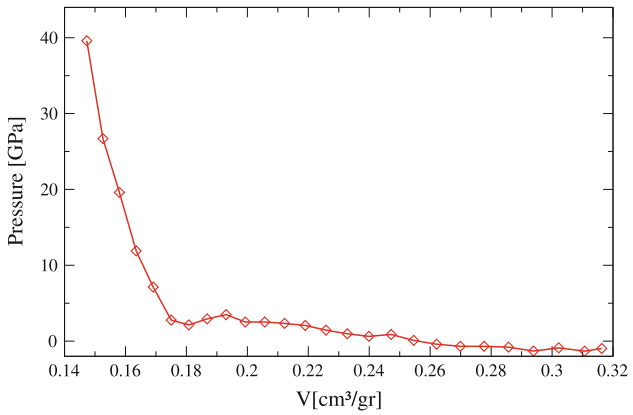

Fig. 2 *P–V* equation of state of amorphous GeO_2

this volume collapse occurs in the region between 3 and 7 GPa, and is associated with a change in the Ge atomic coordination number, from four nearest-neighbor oxygen atoms at low density to six nearest-neighbor oxygen atoms at high density.

Figure 3 displays the partial PDF. It can be seen that the Ge–O bond length increases a little bit, from 1.72 Å at normal pressure to 1.82 Å at high pressure. At the same time, the O–O distance decreases as the pressure increases, and the same trend is seen in the Ge–Ge distances.

Figure 4b shows the angular distribution of Ge and O atoms. We can see that the angle O–Ge–O shifts from 108° at normal pressure to approximate to 90° at high pressure. For the Ge–O–Ge angle the change is more drastic, from 134° to approximate 95°, as the pressure increases.

With this information, in addition to the changes in the coordination number, one can deduce the basic building blocks which compose this glass, from a structural point of view. These structures are mainly GeO_4, GeO_5, and GeO_6. Precisely, Fig. 5 shows the changes suffered in the coordination numbers by these building blocks as the pressure increases. At the beginning, almost the entire sample was composed of GeO_4. Then, at the density of 4.1 g/cm^3 the number of GeO_6 structures starts to increase. The crossover is found at approximately 5.2 g/cm^3, finishing at the end with almost 90% of GeO_6. In summary, the general trend is that the number of GeO_4 tetrahedra monotonically decreases whereas the GeO_6 monotonically increases as pressure increases.

This information allows us to infer that, under an increase in pressure, main structural change occurs in the basic structure of amorphous germania. This change consists of a transition from a sample composed mainly by a tetrahedral basic structure to a sample composed mainly by an octahedral one at high pressure, which is shown in Fig. 6.

Finally, Fig. 7 displays the changes in the vibrational density of states (VDOS) with respect to the pressure. We observe two main bands in the VDOS of germania. At low density we can see a high frequency band, associated mainly with intra-tetrahedron vibration. At high density the low frequency band shows a clear peak, and the high frequency band becomes flatter and wider.

In summary, according to our simulation, there is a short-range order defined by a slightly distorted tetrahedron

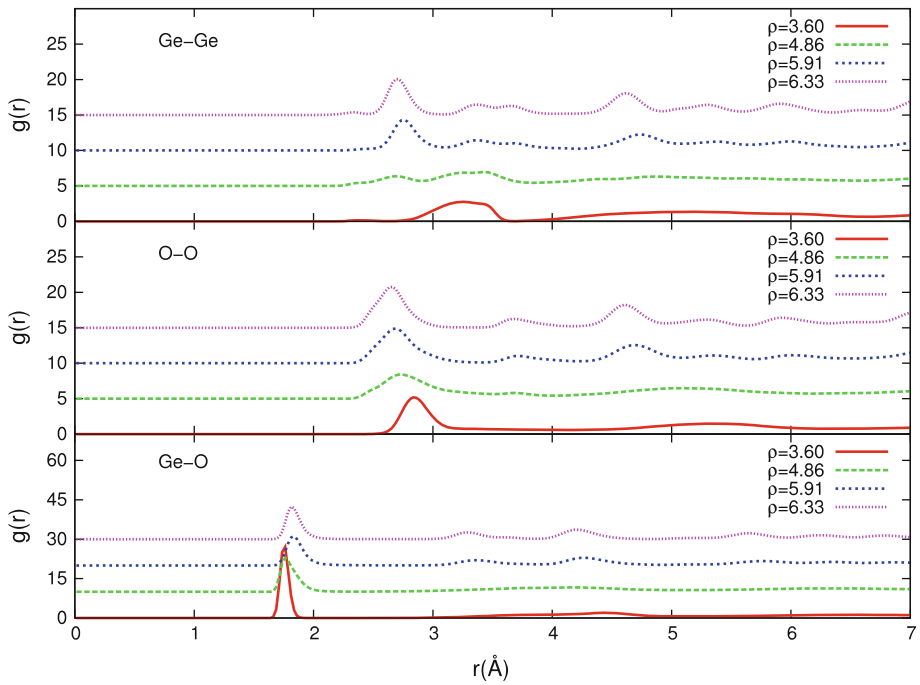

Fig. 3 (Color online) Total and partial pair distribution functions of amorphous GeO_2 at different densities

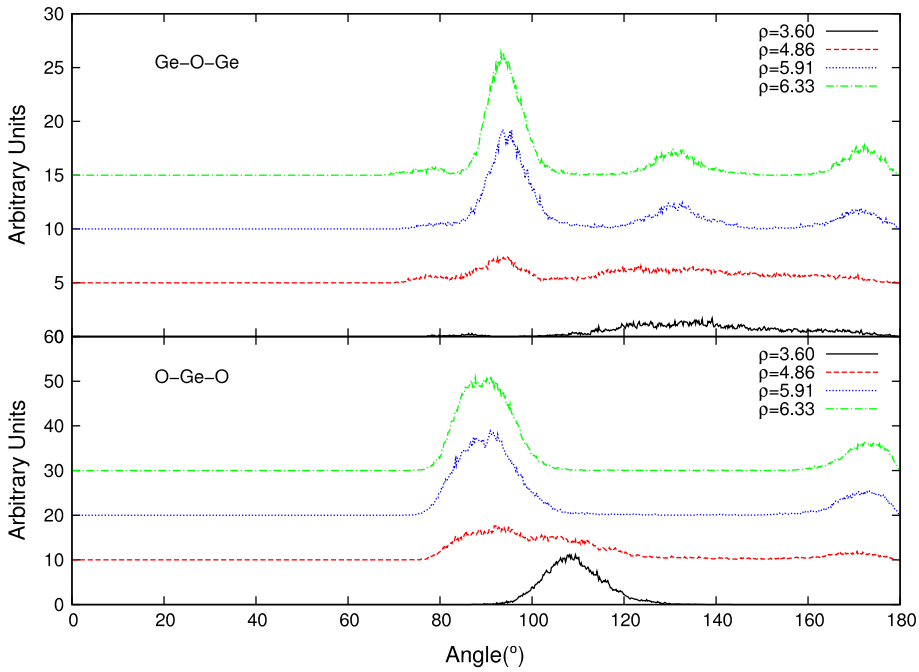

Fig. 4 (Color online) Angular distribution of amorphous GeO_2 at different densities

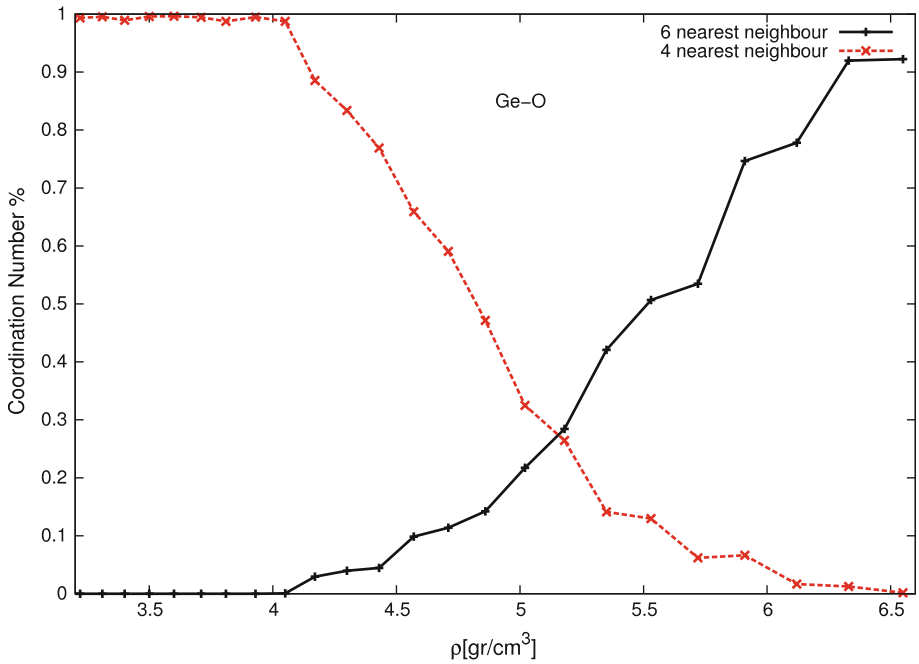

Fig. 5 (Color online) Changes in the coordination numbers in amorphous GeO_2 under pressure

at low density, and a short-range order defined by an octahedron at high density. The structural change occurs between 5 and 9 GPa. The octahedra are linked mainly by corners and edges at high density, in a similar way as the tetrahedra are linked at low density. We can observe two main bands, at low frequency associated to inter-octahedra vibration, and a high frequency bands, associated to intra-octahedron vibration, mainly due to oxygen atoms.

Amorphous Al_2O_3

Aluminum oxide or Alumina, Al_2O_3, is a very important material which has many technological and industrial applications. This is due to its great hardness, high thermal stability, corrosion resistance, chemical inertness, and good electrical insulation. It has a wide range of applications, from electronics, optics, biomedical, and mechanical engineering to catalyst support.

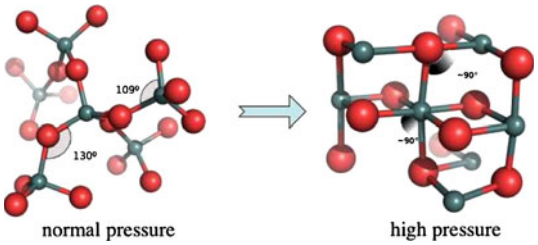

Fig. 6 (Color online) Structural transformation of the basic building blocks from room pressure to high pressure. The transformation takes place between 5–9 GPa. The figures are snapshots from the actual simulation

Alumina exists in a variety of metastable structures, so-called transition phases [17], which are stable in a determinate range of temperature and pressure. For example, the sequence that occurs when temperature increases is amorphous $\rightarrow \gamma \rightarrow \delta \rightarrow \theta \rightarrow \alpha$. At ambient conditions, the stable phase is corundum, α-Al_2O_3.

Amorphous alumina was studied by a combination of classical and first principles MD, employing a supercell of 80 atoms in the microcanonical ensemble. The preparation of the sample was done using classical MD, and the final configuration from this process was used as input for the ab initio MD, following the methodology used for SiO_2 by Benoit et al. [18]. The structural model of amorphous alumina, used as initial configuration for the ab initio MD simulation, was generated by first performing classical MD with a pair-wise interatomic potential [19] which is able to reproduce a number of experimental properties of crystal [19], liquid [20], and amorphous [21] phases. It is interesting to note that, despite the system being rather small, the short-range correlations are basically the same obtained in bigger systems with this interatomic potential [21]. The "quench from the melt" technique used to obtain the amorphous sample follows [21]. The glass sample we obtained in this way, a cubic cell with density $\rho = 3.2$ g/cm^3, was used as input configuration for the ab initio MD. This was done in the framework of Density Functional Theory (DFT) using the total-energy Vienna Ab initio Simulation Package, VASP [22]. For the electronic structure we have chosen the exchange-correlation potential as approximated by the Perdew–Zunger [23] parameterization of the Local Density Approximation (LDA). The valence wave functions were expanded in plane waves at the Γ point of the supercell, using a cut-off of 296.77 eV. The core electrons were replaced by the ultrasoft pseudopotentials (USPP) supplied in the VASP package. The ab initio MD was also performed in the NVE ensemble, using periodic boundaries conditions and a time step of 3 ps. The system was equilibrated during 9 ps at $T = 400$ K. The data used to calculate the structural properties were accumulated on the following 4.5 ps. In order to calculate the dynamical properties such as velocity autocorrelation function (VACF) and VDOS, we performed a longer run, over 30 ps, using the same time step and DFT parameters.

Structural properties are studied by examining atomic correlations described by pair distribution functions, coordination numbers, and angular distributions. Figure 8 shows the results of the total and partial $g_{\alpha\beta}(r)$. In the case of ab initio MD, from the position of the first peak of these curves we can infer the Al–Al, Al–O, and O–O nearest-neighbor distances. We can see that the Al–Al

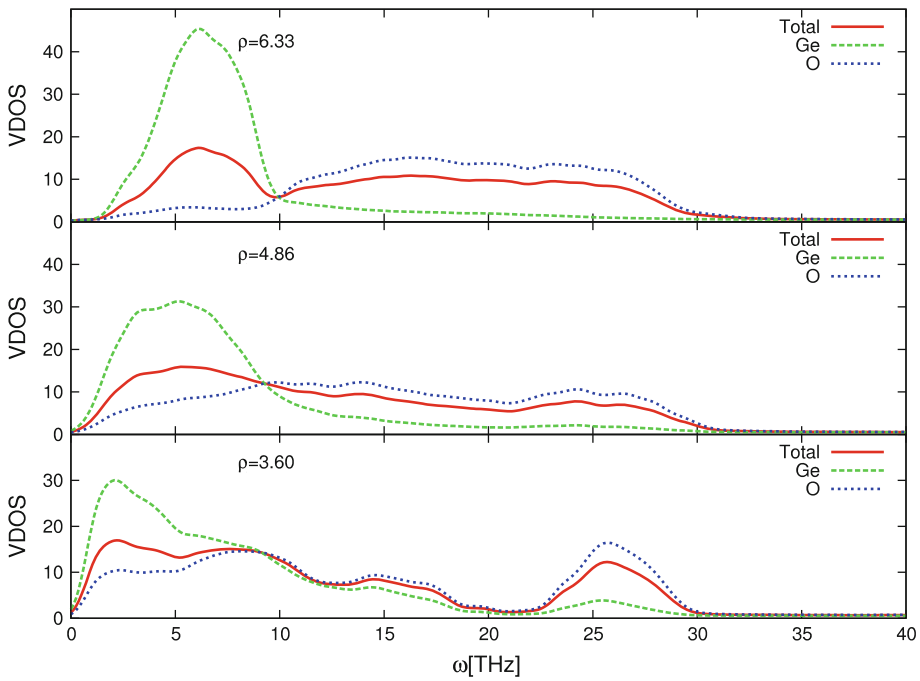

Fig. 7 (Color online) Vibrational density of states of amorphous GeO_2 at different densities

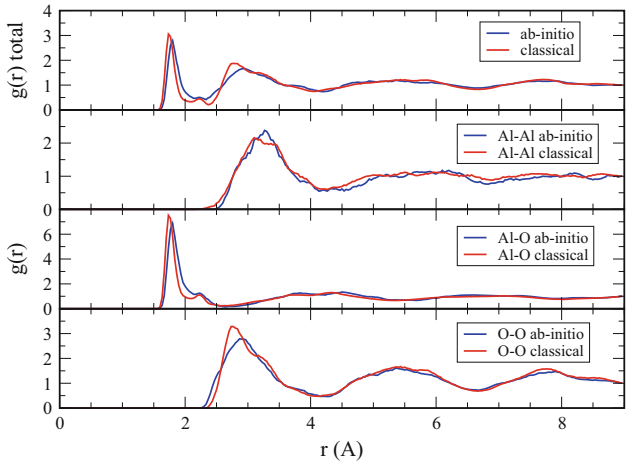

Fig. 8 (Color online) Total and partial pair distribution functions for amorphous Al_2O_3. Classical and ab initio MD simulations

nearest-neighbor distance is 3.14 ± 0.25 Å. In the same way, we can estimate the Al–O bond length to be 1.8 ± 0.1 Å, and the O–O bond length 2.82 ± 0.28 Å. These widths of the first peaks were taken at half the height. These values are slightly different from the ones obtained in classical MD, but closer to the experimental ones. In particular, the Al–O bond length obtained from ab initio MD is in complete agreement with the experimental value of 1.8 ± 0.21 Å.

The bond angle distributions in amorphous Al_2O_3 are depicted in Fig. 9. The expected angles in a AlO_4 tetrahedron, O–Al–O = 109.5°, O–O–O = 60°, and Al–O–O = 35.3° are all predominant in these angle distributions. This leads to the conclusion that such a tetrahedron is one of the basic units in the local amorphous structure, as reported in [21]. But, interestingly, in contrast to previous classical MD simulations [21, 24], the O–Al–O angle

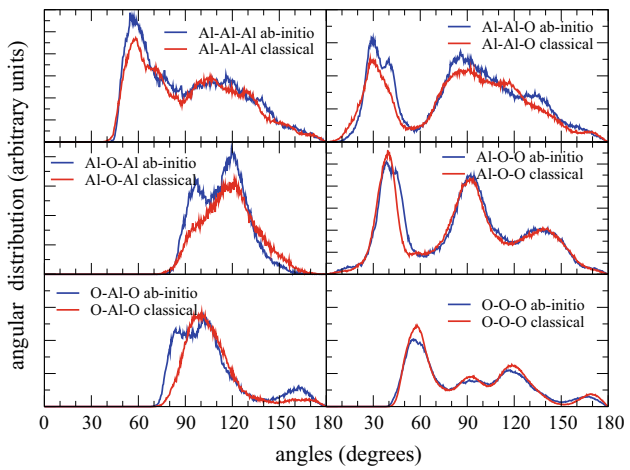

Fig. 9 (Color online) Angular distribution for amorphous Al_2O_3. Classical and ab initio MD simulations

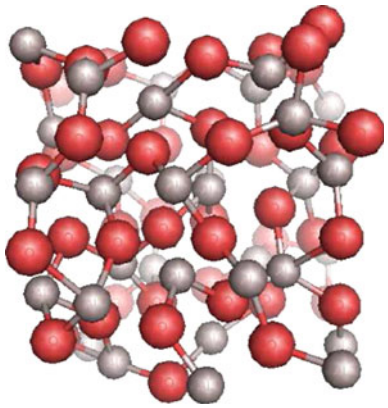

Fig. 10 (Color online) Snapshot of a configuration of amorphous Al_2O_3, obtained by ab initio MD simulations. *Small gray spheres* correspond to aluminum atoms and *big red spheres* to oxygen atoms

distribution also presents a peak around 85°. This piece of information, together with the fact that the average Al–O coordination number is higher than four, and the Al–O bond length is higher than in classical MD, suggests that a certain proportion of distorted AlO_5 and AlO_6 octahedra are also present.

In Fig. 10 we can see a snapshot of the simulation. Figure 11 shows snapshots of the basic structural units and their connectivity. The short-range order is composed by a basic tetrahedron. Regarding the structure beyond the short-range order, we can see that the basic building blocks, tetrahedra and distorted octahedra, are linked to each other not only at 120°, as obtained from classical MD, but also around 95°. This means that these basic units are linked not only by corners, but also by sharing edges and faces.

Regarding the vibrational properties of alumina, the vibrational (or phonon) density of states (v-DOS) has been calculated by ab initio methods for α and θ phases of Al_2O_3 by Lodziana et al. [25], and for γ-Al_2O_3 by Ching et al. [26]. For amorphous Al_2O_3, in Fig. 12 we display our calculation of the v-DOS using ab initio MD, obtained by taking the Fourier transform of the velocity autocorrelation

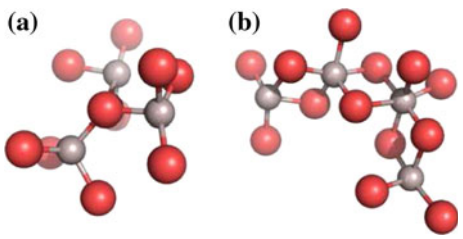

Fig. 11 (Color online) Snapshots of the structural units and their connectivity found in the simulation of amorphous Al_2O_3. **a** Corner-sharing tetrahedra. **b** Edge-sharing polyhedra. In both figures, the *small gray spheres* correspond to aluminum atoms and the *big red spheres* to oxygen atoms

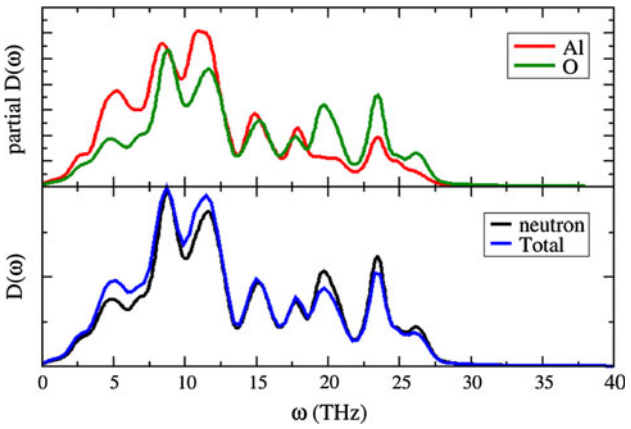

Fig. 12 (Color online) Partial, neutron, and total vibrational density of states for amorphous Al_2O_3. Ab initio MD simulations

function. In Fig. 12a the partial Al and O atoms v-DOS are presented, and Fig. 12b shows the total and the neutron weighted v-DOS. Their general features are that they range from 0 to approximately 30 THz, and two bands can be distinguished, a lower one up to 15–20 THz, and a higher band from 20 to 30 THz. The lower band is mainly due to Al atoms vibrations, whereas the higher band to O atoms, in agreement to the results of Vashishta et al. who used an empirical interatomic potential [24]. The different peaks found in Fig. 12 can be compared to the calculated v-DOS of γ-Al_2O_3 [26]. As is well known, amorphous Al_2O_3 is the precursor of γ-Al_2O_3 and shares many of its structural properties. In fact, the width of the spectra is the same, and the main peaks present at the low and high frequency band may have similar origins. For instance, the two peaks of the Al atoms spectrum, near 8 and 11 THz, could be associated to the corresponding peaks of the Al octahedra ($\sim$250 cm^{-1}) and Al tetrahedra ($\sim$350 cm^{-1}) shown in Fig. 3 of the [26]. Similarly, the peak at 23 THz of O corresponds to the one at 760 cm^{-1} in Fig. 3 of the [26].

A summary of our findings is presented in Table 1. Here we compare the density, the coordination number, and the Al–O bond length to previous calculations, in the liquid and in the amorphous state obtained via classical MD, as well as in different phases of the crystalline state.

Amorphous $CdTeO_3$

In the last years amorphous CdTe oxide thin films have been extensively studied [29–37], mainly because this material could play in CdTe solar cells technology a similar role to that of SiO_2 in Si technology. Native oxides have also been identified on CdTe surfaces [38]. Recently, this material doped with indium has been proposed as a transparent conducting oxide and transparent oxide semiconductor [39].

Table 1 Comparison of structural properties among different phases of alumina

Phase	Density (g/cm^3)	Al coordination number	Bond length (Å)
	3.17	4 (76%), 5 (22%)	1.76
Amorphous, classical MD[a]	3.90	4 (23%), 5 (51%), 6 (21%)	1.77
	4.20	4 (15%), 5 (21%), 6 (64%)	1.79
Amorphous, ab initio MD[b]	3.17	4 (50%), 5 (42%), 6 (5%)	1.81
Liquid, classical MD[c]	3.17	3 (13%), 4 (66%), 5 (20%)	1.71
γ, ab initio[d]	3.66	4 (37%), 6 (63%)	1.94 ± 0.3
θ	3.65	5 (50%), 6 (50%)	1.9 ± 0.3
α	3.98	6 (100%)	1.97

[a] [21], unpublished (2008)

[b] Submitted (2009)

[c] [20]

[d] [27, 28]

Most of the experimental works on the amorphous oxidized CdTe thin films up to date have been devoted to the optimization of growth techniques [29, 30, 33, 37], but almost nothing is known about the structure of the amorphous phases. We have used ab initio MD to find amorphous $CdTeO_3$ structural units. The structural units of crystalline $CdTeO_3$ are distorted TeO_3 trigonal pyramids that are linked to each other with Cd atoms. This arrangement is similar to the one found in tellurite glasses [40, 41]. There are Cd and Te atoms each of which occupy two non-equivalent sites, and O atoms in six non-equivalent sites. Both Cd atoms are sixfold coordinated with Cd–O bond lengths in the 2.197–2.476 Å range. The bond angles deviate as much as 31° from the ideal octahedral bond angles of 90° and 180°. O atoms always link one Te atom with one, two, or three Cd atoms, and the average coordination of O atoms is three.

The ab initio MD simulations were made using the DFT with the PBE parameterization, as implemented in the PWSCF code of the Quantum-ESPRESSO package [42]. The interatomic forces have been calculated using the Hellmann–Feynman theorem on the self-consistent electronic ground state at each time step. The first Brillouin zone has been sampled using only the Γ -point. A gaussian smearing has been applied to the density of states to avoid convergence problems, with a smearing parameter of 0.02 Ry. A plane-wave basis set has been used, with kinetic energy cut-offs of 30 and 180 Ry for the expansion of the wave functions and the charge density, respectively. The

electron–ion interaction has been treated in the pseudopotential approximation. We used the existing pseudopotentials for Cd and O, and generated a new one for Te, which are available in [43]. The sample was prepared by starting with a configuration where the atoms were located at random non-overlapping positions. Then we run a MD, with velocity rescaling at every step to keep the temperature fixed at 3,000 K, in order to lose correlations with the starting configuration. After that, the temperature is lowered using the Berendsen thermostat, down to 300 K [45]. Recently has been shown that the structural model of amorphous $CdTeO_3$ and other related compounds obtained in this way reproduce the XPS spectra [44].

Figure 13 shows the PDF of a $CdTeO_3$ and the contributions of the partial PDFs. The first and second coordination shells display average bond lengths of 1.97 Å (Te–O bonds) and 2.25 Å (Cd–O bonds). The other peaks in the PDF correspond to geometrical correlations that are too far to be chemical bonds. The static structure factor, $S(q)$, as defined in Eq. 4, could be compared directly to experiments. In Fig. 14 we display the partials $S(q)$ for the different correlation pairs.

Figure 15 shows the most frequent structural units found in crystal (a) and amorphous (b) $CdTeO_3$. In the amorphous state, Cd is coordinated by either six (1) or five (2) O atoms. Cd may also have a Cd neighbor within the cut-off distance of 3.19 Å. Te atoms are located at the apices of trigonal pyramids (3) or bipyramids (4), like in crystalline TeO_2 and $CdTeO_3$. The cluster (4) is similar to the case of α-TeO_2. Both in α-TeO_2 and amorphous $CdTeO_3$, cluster (4) has two additional O atoms nearby that are not chemically bound to Te [46]. Also, in amorphous $CdTeO_3$, there are some TeO_4 bipyramids with symmetric equatorial bonds, and other bipyramids that have one very long bond and three smaller bonds, indicating that a TeO_3 trigonal pyramid is the chemical unit. These basic units [cluster (3) and (4)] may also have a Cd or Te neighbor within the cut-off distance of 3.19 Å. O atoms can be found in tetrahedral environments, coordinated by one Te and three Cd, or two Te and two Cd. Te is also found three-coordinated by one (or two) Te and two (or one) Cd. Finally, there is a small fraction of O atoms without Cd neighbors, bound to two Te atoms.

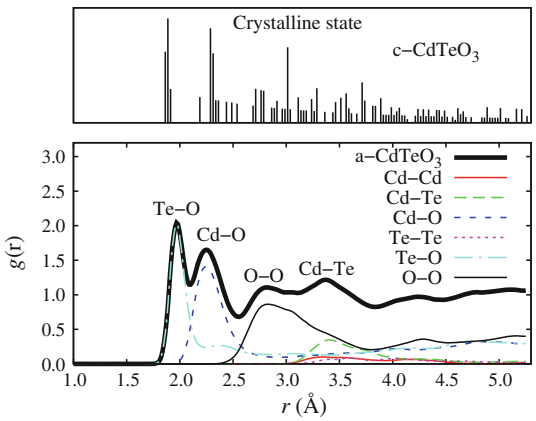

Fig. 13 (Color online) Total and partial pair distribution functions of amorphous $CdTeO_3$. The one at the very top corresponds to the crystalline phase

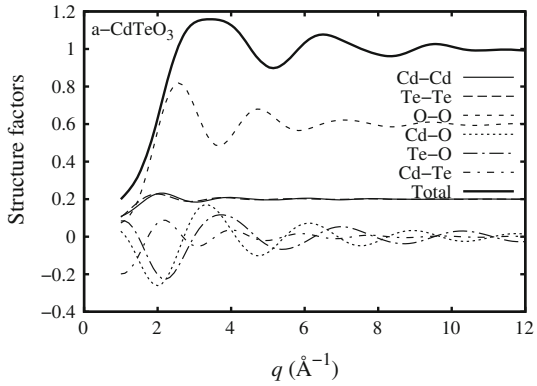

Fig. 14 Partial static structure factors for amorphous $CdTeO_3$

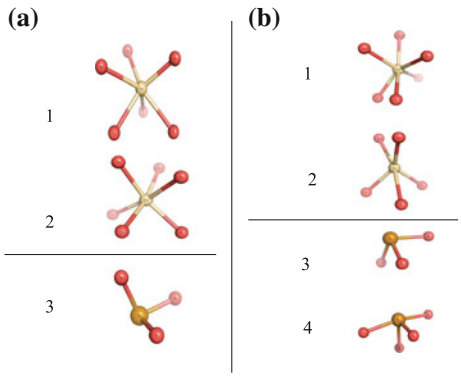

Fig. 15 (Color online) Typical atomic environments in $CdTeO_3$. **a** crystal and **b** amorphous. *Red spheres* represent O atoms. The sphere at the center in clusters (*1*) and (*2*) corresponds to Cd atoms, and the sphere at the center in clusters (*3*) and (*4*) corresponds to Te atoms

We also compute the coordination numbers. Cd atoms are mainly coordinated by five (32%) or six (61%) O atoms, Te atoms are coordinated by three (60%), and four (38%) O atoms. O atoms are coordinated by one (82%) or two (16%) Te atom and a one to three Cd atoms (26, 45, and 21%). There is a residual fraction of O atoms that are not connected to either Cd or Te. In average, Cd atoms are surrounded by 5.7 O atoms, Te atoms are surrounded by 3.4 O atoms, and O atoms are surrounded by 1.9 Cd atoms and 1.0 Te atom.

Conclusions

We have reviewed different applications of MD calculations on complex materials, like binary and ternary

amorphous compounds. As it has been shown, classical MD can be successfully used when good interatomic potentials exist, as in the case of covalent materials like SiO_2 or GeO_2. However, for more complex systems, as Al_2O_3 or a ternary compound like $CdTeO_3$, it is not an easy task to build an interatomic potential, and then ab initio MD should be employed. The MD presented here for amorphous GeO_2 shows that classical MD with a good interatomic potential can model even a structural transformation under pressure, giving atomic level information of the process. The second example presented, the simulation of amorphous alumina, shows the similarities and the differences between classical and ab initio MD. Although in general both results agree regarding the structural properties, some differences were found: in ab initio MD the Al–O bond length is larger than in classical MD, showing better agreement with the experimental results. Finally, we presented an ab initio MD simulation for amorphous $CdTeO_3$, displaying the great diversity of basic building blocks present in this compound. Thus, this atomic level description gives a hint about the difficulty to have an empirical interatomic potential for this kind of compounds.

Acknowledgements This study has been supported by grant Anillo "Computer simulation lab of nano-bio systems" ACT-ADI 24/2006-Chile. We thank our collaborator Paolo Gianozzi. We also acknowledge computer time from different institutions: CINECA-Italy, the Abdus Salam International Centre for Theoretical Physics ITCP-Trieste, the Center of Bioinformatics and Molecular Simulation of the University of Talca-Chile, and MAIDROC Computer Lab and CESMEC, both from Florida International University-Miami. However, most of the calculations have been done in our in-house facilities, thanks to continuous grants from Fondecyt-Chile along these years.

References

1. Cusack NE (1987) The physics of structurally disordered matter: an introduction. Graduate student series in Physics Institute of Physics Publishing, Bristol
2. Zallen R (2004) The physics of amorphous solids. Wiley-VCH, Germany
3. Boolchand EP (2000) Insulating and semiconductors. World Scientific Publishing, Singapore
4. Drabold DA (2009) Eur Phys J B 68:1
5. Allen M, Tildesley D (1987) Computer simulation of liquids. Clarendon Press, Oxford
6. Rappaport DE (1996) The art of molecular dynamics simulation. Cambridge University Press, Cambridge
7. Oeffner RD, Elliott SR (1998) Phys Rev B 58(22):14791
8. Kohanoff J (2006) Electronic structure calculations for solids and molecules: theory and computational methods. Cambridge
9. Marx D, Hutter J (2000) In: Grotendorst J (eds) Modern methods and algorithms of quantum chemistry. NIC series, FZ Jülich, pp 301–409
10. Lorch E (1969) J Phys C Solid State Phys pp 229–237
11. Loong CK, Vashishta P, Kalia RK, Ebbsjö I (1995) Europhys Lett 31(4):201
12. Las Palmeras Molecular Dynamics, see http://www.gnm.cl/lpmd.
13. Smith KH, Shero E, Chizmeshya A, Wolf GH (1995) J Chem Phys 102:6851
14. Peralta J, Gutiérrez G, Rogan J (2008) J Phys Condens Matter 20:145215
15. Refson K (1998) MOLDY, a general—purpose molecular dynamics code. Available free for academic purpose at http://www.earth.ox.ac.uk/~keith/moldy.html, Release 2.13, 1998
16. Sampath S, Benmore CJ, Lantzky KM, Neuefeind J, Leinenweber K, Price DL, Yarger JL (2003) Phys Rev Lett 90(11):115502
17. Wefers K, Misra C (1987) Oxides and hydroxides of aluminum. Alcoa Tech. Pap. 19. Alcoa Laboratories, St. Louis, MO
18. Benoit M, Ispas S, Jund P, Jullien R (2000) Eur Phys J B 13:631
19. Matsui M (1996) Phys Chem Min 23:345
20. Gutiérrez G, Belonoshko AB, Ahuja R, Johansson B (2000) Phys Rev E 61:2723
21. Gutiérrez G, Johansson B (2002) Phys Rev B 65:104202
22. Kresse G, Furthmüller J (1996) Phys Rev B 54:11169
23. Perdew JP, Zunger A (1981) Phys Rev B 23:5048
24. Vashishta P, Kalia RK, Nakano A, Rino JP (2008) J Appl Phys 108:083504
25. Lodziana Z, Parlinski K (2003) Phys Rev B 67:174106
26. Ching WY, Ouyang L, Rulis P, Yao H (2008) Phys Rev B 78:014106
27. Gutiérrez G, Taga A, Johansson B (2002) Phys Rev B 65:012101
28. Menéndez E, Gutiérrez G (2005) Phys Rev B 72:035116
29. Espinoza-Beltrán FJ, Zelaya O, Sánchez-Silencio F, Mendoza-Álvarez JG, Farias MH, Baños L (1993) J Vac Sci Technol A 11:3062
30. Zapata-Navarro A, Zapata-Torres M, Sosa V, Bartolo-Pérez P, Peña JL (1994) J Vac Sci Technol A 12:714
31. Iribarren A, Menéndez-Proupin E, Caballero-Briones F, Castro-Rodríguez R, Peña JL (1999) J Appl Phys 86:4688
32. Caballero-Briones F, Zapata-Navarro A, Bartolo-Pérez P, Rodríguez RC, Zapata-Torres M, Cauich W, Peña JL (1998) Rev Mex Fis 44:268
33. Azhari MYE, Azizan M, Bennouna A, Outzourhit A, Ameziane E, Brunel M (2000) Thin Solid Films 366:82
34. Arizpe-Chávez H, Ramírez-Bon R, Espinoza-Beltrán F, Zelaya-Angel O, Marín J, Riera R (2000) J Phys Chem Solids 61:511
35. Iribarren A, Menéndez-Proupin E, Caballero-Briones F, Castro-Rodríguez R, Peña JL (2001) Mod Phys Lett B 15:643
36. Bartolo-Pérez P, Rodríguez RC, Caballero-Briones F, Cauich W, Peña JL, Farias MH (2002) Surf Coat Technol 155:16
37. Castro-Rodríguez R, Iribarren A, Bartolo-Pérez P, Peña JL (2005) Thin Solid Films 484:100
38. Miotto R, Kiss FD, Ferraz AC (2003) Surf Sci 525:24
39. Castro-Rodríguez R, Peña JL, Leccabue F, Watts BE, Melioli E (2005) Appl Phys Lett 87:061916
40. Ushino T, Yoko T, (1996) J Non-Cryst Solids 204:243
41. Sekiya T, Mochida N, Oshtsuka A, Tonokawa M (1992) J Non-Cryst Solids 144:128
42. Baroni S, Corso AD, de Gironcoli S, Giannozzi P, Cavazzoni C, Ballabio G, Scandolo S, Chiarotti G, Focher P, Pasquarello A, Laasonen K, Trave A, Car R, Marzari N, Kokalj A (2005) QUANTUM ESPRESSO package. http://www.quantum-espresso.org/
43. Cd.pbe-n-van.UPF, O.pbe-rrkjus.UPF and Te.pbe-rrkj.UPF at http://www.quantum-espresso.org/pseudo.php
44. Amézaga A, Holmstrom E, Lizárraga R, Menéndez-Proupin E, Bartolo-Pérez P, Giannozzi P (2010) Phys Rev B 81:014210
45. Menéndez-Proupin E, Gianozzi P, Peralta J, Gutiérrez G (2009) Phys Rev B 79:014205
46. Menéndez-Proupin E, Gutiérrez G, Palmero E, Peña JL (2004) Phys Rev B 70:035112